




Broadband coherent optical memory based on electromagnetically induced transparencyYan-Cheng Wei ^{1,2}, Bo-Han Wu,¹ Ya-Fen Hsiao,¹ Pin-Ju Tsai ^{1,2} and Ying-Cheng Chen ^{1,3,*}¹*Institute of Atomic and Molecular Sciences, Academia Sinica, Taipei 10617, Taiwan*²*Department of Physics, National Taiwan University, Taipei 10617, Taiwan*³*Center for Quantum Technology, Hsinchu 30013, Taiwan*

(Received 18 September 2020; accepted 29 November 2020; published 24 December 2020)

Quantum memories, devices that can store and retrieve photonic quantum states on demand, are essential components for scalable quantum technologies. It is desirable to push the memory towards the broadband regime in order to increase the data rate. Here, we present a theoretical and experimental study of broadband optical memory based on the electromagnetically induced transparency (EIT) protocol. We first provide a theoretical analysis of the issues and requirements needed to achieve broadband EIT memory. We then present our experimental efforts for the movement of EIT memory in cold atoms towards the broadband or short-pulse regime. A storage efficiency of $\sim 80\%$ with a pulse duration of 30 ns (corresponding to a bandwidth of 14.7 MHz) is realized. Due to limitations of the available intensity of the control beam, we could not achieve an optimal storage for the even shorter pulses but were still able to obtain an efficiency of greater than 50% with a pulse duration of 14 ns (31.4 MHz). The time-bandwidth product achieved at an efficiency of 50% is 1267(89).

DOI: [10.1103/PhysRevA.102.063720](https://doi.org/10.1103/PhysRevA.102.063720)**I. INTRODUCTION**

Quantum memories are crucial components in linear-optics-based quantum computation and long-distance quantum communication based on the quantum repeater protocol [1,2]. Significant efforts and progress have been made for the development of quantum memories over the past two decades. The parameters used to evaluate the performance of a quantum memory include the fidelity, efficiency, storage time, bandwidth or capacity, and noise level. The development of a quantum memory with a high performance in all aspects remains a great challenge. In this work, we focus our discussion on achieving a broad bandwidth while maintaining a high efficiency for coherent optical memories based on the electromagnetically induced transparency (EIT) protocol.

Optical memory based on the off-resonant Raman transition is generally considered to be advantageous to achieving a high bandwidth. The Raman memory protocol has been utilized in many works to push the bandwidth towards ~ 100 MHz – 1 GHz range with an efficiency ranging from ~ 10 –30% [3–8]. In a recent work the same protocol has been applied to achieve an efficiency of 82% at a bandwidth of ~ 100 MHz [9].

The on-resonant two-photon transition in a Λ -type atomic system also allows for the implementation of broadband optical memory, as long as the optical depth of the media is high and the intensity of the control beam is strong enough [10–13]. The character of the memory is quite different depending on the ratio of the spectral bandwidth of the probe pulse (denoted as B) to the EIT transparent bandwidth ($\Delta\omega_{\text{EIT}}$). If B is equal to or larger than $\Delta\omega_{\text{EIT}}$, the memory operation involves coher-

ent absorption of the probe pulse by the two Autler-Townes absorption peaks, which is called the Autler-Townes-splitting (ATS) protocol [12–14]. The light-matter interaction under such a condition is nonadiabatic and involves an oscillation between the optical coherence and the collective ground-state coherence (also called spin wave). In the opposite case ($B < \Delta\omega_{\text{EIT}}$), the memory operation is an EIT protocol which relies on adiabatic elimination of the absorption and coherent transfer between the optical field and the collective atomic spin wave. The features of and differences between the EIT and ATS protocols have been well studied [10,12,13]. One earlier study has proposed a scheme for broadband storage using EIT protocol with matched Fourier components for the probe and control laser beams [15]. Experimentally, a bandwidth of 14.7 MHz with an efficiency of 8.4% has been demonstrated using the ATS protocol [12]. An efficiency of up to 92% has been obtained using the EIT protocol, but the bandwidth is only up to 2.2 MHz [16–18].

In this paper, we explore the issues and requirements that need to be resolved in order to extend the bandwidth of adiabatic EIT memories. Aside from efficiency, we invoke another important figure of merit for a memory: the waveform likeness (WL) [16,18,19], which quantifies the degree of distortion of a probe pulse. In the single-photon regime, the waveform likeness is related to the overlap of the temporal mode of the photons with and without storage, which is crucial in some applications of quantum memory. We show that waveform likeness can be considered as an experimental parameter to evaluate the degree of adiabaticity of a memory. For a steady-state EIT spectrum, we identify that it can be categorized into two regimes in which the EIT transparent bandwidth is proportional to the intensity or field amplitude of the control field, for low and strong control fields, respectively. We term these two regimes the intensity-linear or field-linear EIT

*Corresponding author: chenyc@pub.iams.sinica.edu.tw

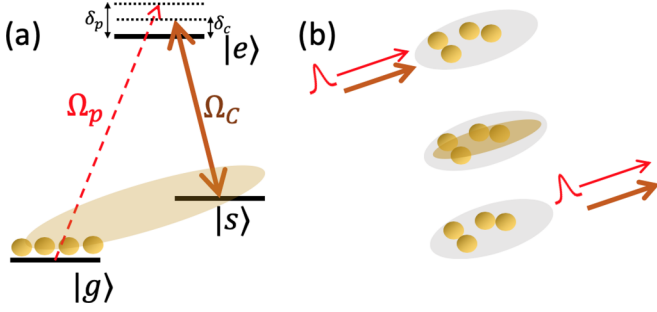


FIG. 1. (a) Transition scheme of the Λ -type EIT system. $|g\rangle$ and $|s\rangle$ are the two ground states and $|e\rangle$ is the excited state. $\Omega_{p,c}$ stand for the Rabi frequency of the probe and the control field, respectively. (b) Photonic storage through the EIT protocol. In both graphs, the yellow shaded area denotes the spin coherence in the two ground states.

bandwidth regime. For a pulsed probe case, we show that EIT memory can be categorized into the narrowband or broadband regime, with $B < \Gamma$ or $B \geq \Gamma$, respectively, where Γ is the spontaneous decay rate of the probe transition. We show that EIT memory is limited by the efficiency in the narrowband regime and by the waveform likeness in the broadband regime. We clarify that a high efficiency and a high waveform likeness can be maintained for EIT memory even in the broadband regime. The quantitative requirements to achieve such high-performance storage are given. Our theoretical study provides essential physical insight for the implementation of a broadband EIT memory.

We also present experimental efforts aimed toward producing a broadband EIT memory. We achieve a storage efficiency of $\sim 80\%$ for probe pulses with a full width at half maximum (FWHM) temporal duration (T_p) of 30 ns, which corresponds to a bandwidth of 14.7 MHz. Limited by the available control intensity, we cannot achieve the optimized efficiency for $T_p < 30$ ns but are still able to obtain an efficiency above 50% for $T_p = 14$ ns (31.4 MHz). The time-bandwidth product (TBP), defined as the ratio of the storage time at 50% storage efficiency to the FWHM duration (T_p) of the input probe pulse, is an important figure of merit for memory applications. We achieve a TBP of 1267(89).

II. THEORETICAL STUDY OF BROADBAND EIT STORAGE

The transition scheme of the Λ -type system for EIT storage is shown in Fig. 1(a). The population is assumed to be prepared in the ground state, $|g\rangle$. The weak probe field, to be stored and retrieved on demand, drives the $|g\rangle \leftrightarrow |e\rangle$ transition with a Rabi frequency of Ω_p . The control field, with a Rabi frequency of Ω_c , drives the $|s\rangle \leftrightarrow |e\rangle$ transition.

Under the rotating-wave approximation, the system Hamiltonian can be described by

$$\hat{H} = -\delta_p \hat{\sigma}_{ee} - \delta_2 \hat{\sigma}_{ss} + \frac{1}{2}(\Omega_p \hat{\sigma}_{eg} + \Omega_c \hat{\sigma}_{es} + \text{H.c.}), \quad (1)$$

where $\hat{\sigma}_{ij} \equiv |i\rangle \langle j|$ denotes the atomic operator, $\delta_{p,c}$ denotes the one-photon detunings of the probe and control field, respectively, and $\delta_2 = \delta_p - \delta_c$ denotes the two-photon detuning.

Theoretical analysis based on the Maxwell-Schrödinger equation (MSE) and the optical Bloch equations (OBEs) is carried out. Under the weak-probe perturbation, the relevant equations are

$$\partial_t \sigma_{eg} = (i\delta_p - \gamma_{ge})\sigma_{eg} + \frac{i}{2}\Omega_c \sigma_{sg} + \frac{i}{2}\Omega_p, \quad (2)$$

$$\partial_t \sigma_{sg} = (i\delta_2 - \gamma_{sg})\sigma_{sg} + \frac{i}{2}\Omega_c^* \sigma_{eg}, \quad (2)$$

$$\left(\frac{1}{c}\partial_t + \partial_z\right)\Omega_p = i\frac{D\Gamma}{2L}\sigma_{eg}, \quad (3)$$

where D and L denote the optical depth and the length of the atomic media, respectively [17]. γ_{ge} is the decay rate of the optical coherence σ_{eg} , and it is $\Gamma/2$ if spontaneous decay is the only relaxation mechanism. γ_{sg} is the ground-state decoherence rate.

A. Spectral response

Equations (2) and (3) can be easily solved in the frequency domain (ω space) by Fourier transformation [17]. We consider the continuous-wave control field with a constant amplitude. Due to the weak-probe approximation, its depletion inside the medium is negligible. Therefore, the Rabi frequency of the control field is treated as a constant. Without loss of generality, we also consider Ω_c to be a real number. The ω -space probe field can be obtained as follows:

$$W_p(\omega, z) = W_p(\omega, 0) \exp[ik(\omega)z], \quad (4)$$

where

$$k(\omega) = \frac{\omega}{c} + \frac{D\Gamma}{4L} \frac{\omega}{i\omega[i(\omega + \delta_p) - \frac{\Gamma}{2}] + \frac{\Omega_c^2}{4}} \equiv k_0(\omega) + k_1(\omega), \quad (5)$$

where $k_0(\omega) = \omega/c$ is the free-space wave number, $k_1(\omega)$ is the spectral response function of the EIT medium, and $W_p(\omega, 0)$ is the spectral amplitude of the input probe pulse. For simplicity, we assume $\delta_c = 0$ and the ideal case with $\gamma_{sg} = 0$. For steady-state probe transmission, we can set $\omega = 0$ and obtain $T(\delta_p) = \exp\{-2 \text{Re}[k(\delta_p)L]\}$. The FWHM bandwidth of the EIT transparent window ($\Delta\omega_{\text{EIT}}$) is an important parameter and can be obtained by

$$\Delta\omega_{\text{EIT}} = \sqrt{\frac{D - \ln(2) + 2 \ln(2)(\Omega_c^2/\Gamma^2) - \sqrt{g(D, \Omega_c)}}{2 \ln(2)}} \Gamma, \quad (6)$$

where

$$g(D, \Omega_c) = [D - \ln(2)][D - \ln(2) + 4 \ln(2)(\Omega_c^2/\Gamma^2)]. \quad (7)$$

The relationship between $\Delta\omega_{\text{EIT}}$ and Ω_c is depicted in Fig. 2(a). In the weak-control regime ($\Omega_c \ll \sqrt{D}\Gamma$), the EIT transparent bandwidth is [17]

$$\Delta\omega_{\text{EIT}} \approx \sqrt{\ln(2)} \frac{\Omega_c^2}{\sqrt{D}\Gamma}. \quad (8)$$

The EIT transparent bandwidth is linearly proportional to Ω_c^2 or the control intensity, so we term it the intensity-linear bandwidth regime. In the strong-control regime ($\Omega_c \gg \sqrt{D}\Gamma$), $\Delta\omega_{\text{EIT}} \approx \Omega_c$, which scales linearly with the control field amplitude, so we term it the field-linear bandwidth regime. By

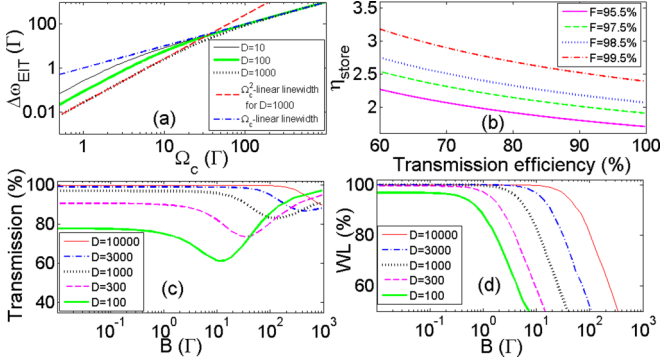


FIG. 2. (a) The black thin-solid, green thick-solid, and black dotted curves denote the FWHM EIT transparent bandwidth ($\Delta\omega_{\text{EIT}}$) versus Ω_c for optical depths D of 10, 100, and 1000, respectively. The red dashed and blue dash-dotted lines indicate the approximate values of $\Delta\omega_{\text{EIT}}$ in the intensity-linear bandwidth regime for $D = 1000$ and the field-linear bandwidth regime, respectively. (b) The η_{store} for the required TE to achieve F of a given value is plotted. $F = 99.5\%$, 98.5% , 97.5% , 95.5% for the curves from top to bottom. (c) and (d) depict TE and WL versus the different bandwidths of the input probe pulse (B) for various optical depths. Here, the Ω_c for different D are determined by $\eta = 2.43$.

setting $\Delta\omega_{\text{EIT}}$ equal to each other for both regimes, the transition Ω_c between these two regimes can be estimated to be $\Omega_c \approx 1.7\sqrt{D}\Gamma$. This justifies our definition of weak or strong control regime and explains the trend in Fig. 2(a) where the intensity-linear regime is wider for a larger optical depth. It should be pointed out that intensity-linear or field-linear regime does not necessarily correspond to the EIT or ATS protocol for the memory [20]. As mentioned in the Introduction, the relative ratio of the bandwidth of the probe pulse (B) to the EIT transparent bandwidth ($\Delta\omega_{\text{EIT}}$) determines the EIT or ATS regime. The intensity-linear or field-linear bandwidth regime does not necessarily determine the broadband or narrowband EIT storage regime. The broadband or narrowband EIT storage depends on the relative ratio between B and Γ , as will be explained later.

B. Pulsed probe fields

In real applications, one needs to store optical probe pulses of a finite bandwidth, instead of a continuous wave. We consider probe pulses with a temporal Gaussian profile with an intensity FWHM duration of T_p . In the frequency domain, the Rabi frequency of the probe pulse reads

$$W_p(\omega, 0) = \frac{T_p \Omega_{p0}}{\sqrt{4 \ln(2)}} \exp\left(-\frac{\omega^2 T_p^2}{8 \ln(2)}\right), \quad (9)$$

where Ω_{p0} is the peak Rabi frequency of the input probe pulse in the time domain. The FWHM bandwidth B of the probe pulse in ω space is $B = \frac{4 \ln(2)}{T_p}$. We consider the on-resonance case for the probe and control fields ($\delta_p = \delta_c = 0$) and the ideal case with $\gamma_{sg} = 0$ and $\gamma_{ge} = \frac{\Gamma}{2}$. For the general case, readers can refer to Ref. [17].

The solution of the slow light pulse in the time domain can be obtained using Eqs. (4), (5), and (9) and Fourier transforming the probe pulse back to the time domain as

follows [17]:

$$\Omega_p(t, z = L) = \frac{1}{\sqrt{2\pi}} \int_{-\infty}^{\infty} d\omega e^{-i\omega t} W_p(\omega, 0) e^{ik(\omega)L}. \quad (10)$$

Applying a Taylor expansion of $k_1(\omega)$ with respect to ω , one obtains the dispersion terms of an EIT medium,

$$k_1(\omega) = \sum_n a_n \omega^n \quad a_1 = \frac{D\Gamma}{\Omega_c^2 L}, \quad a_2 = i \frac{2D\Gamma^2}{\Omega_c^4 L},$$

$$a_3 = \frac{4D\Gamma(\Omega_c^2 - \Gamma^2)}{\Omega_c^6 L}, \quad a_4 = i \frac{8D\Gamma^2(2\Omega_c^2 - \Gamma^2)}{\Omega_c^8 L}, \quad (11)$$

where the explicit forms of the dispersion terms up to $O(\omega^4)$ are written down. The dispersion term $O(\omega)$ is related to group delay [17], which reads

$$T_d = \frac{L}{v_g} = \frac{L}{c} + \frac{D\Gamma}{\Omega_c^2}, \quad (12)$$

where v_g is the group velocity of the probe pulse in the EIT medium [17]. For the later use, we define a parameter η by

$$\eta \equiv \frac{D\Gamma}{\Omega_c^2 T_p}. \quad (13)$$

When $v_g \ll c$, $\eta \approx T_d/T_p$. It should be noted that the term L/c in T_d may not be negligible in the short pulse regime. $O(\omega^2)$ and $O(\omega^3)$ are related to pulse broadening and pulse asymmetry, respectively [17,21]. The ratio of the absolute value of $O(\omega^3)$ to $O(\omega^2)$ for a pulse of bandwidth B is

$$\left| \frac{O(\omega^3)}{O(\omega^2)} \right| = \frac{|\Omega_c^2 - \Gamma^2| B}{\Omega_c^2 \Gamma}. \quad (14)$$

If this ratio is negligible one can keep up to the $O(\omega^2)$ term only, and an analytic form of the probe pulse solution can be obtained. The details can be found in [17]. In the general case, the slow light transmission efficiency (TE) can be exactly calculated by

$$\text{TE} = \frac{\int d\omega |W_p(\omega, 0)|^2 \exp\{-2z \text{Im}[k(\omega)]\}}{\int d\omega |W_p(\omega, 0)|^2}. \quad (15)$$

The ratio $|O(\omega^3)/O(\omega^2)|$ in Eq. (14) is smaller than $(1 + \frac{\Gamma^2}{\Omega_c^2}) \frac{B}{\Gamma} = [\frac{B}{\Gamma} + 4 \ln(2) \frac{B}{D}]$, where Eq. (13) is used. We focus our discussion on EIT memory in the high optical depth regime (e.g., $D > 100$) and η is chosen around 2–3, as will be discussed later. Therefore, $\frac{B}{D} \ll 1$ is valid. In the narrowband regime, $B \ll \Gamma$ and thus $|O(\omega^3)/O(\omega^2)| \ll 1$. The formulation for keeping the dispersion up to the $O(\omega^2)$ term is already a good approximation. On the other hand, in the broadband EIT storage regime ($B \gg \Gamma$), the $O(\omega^3)$ term could be larger than the $O(\omega^2)$ term and should be considered, which may lead to pulse distortion. We next consider the contribution of even higher order dispersion terms in the broadband EIT regime. Note that the ratio of the higher order even and odd dispersion terms, $O(\omega^{2n+2})/O(\omega^{2n})$ and $O(\omega^{2n+3})/O(\omega^{2n+1})$ with $n = 1, 2, 3, \dots$, is $\approx (\frac{B}{\Omega_c})^2$. Since we consider the storage in the EIT protocol, the condition $B < \Delta\omega_{\text{EIT}}$ is valid. From Fig. 2(a), we know that $\Delta\omega_{\text{EIT}} < \Omega_c$ is always valid. Thus, $(\frac{B}{\Omega_c})^2 < (\frac{B}{\Delta\omega_{\text{EIT}}})^2 \ll 1$ is valid. A reasonable approxi-

mation can be obtained by neglecting the dispersion terms of $O(\omega^4)$ and higher.

In the EIT memory protocol, the control field is turned off adiabatically to convert the optical probe field into a collective atomic spin wave and then retrieves the optical field by turning on the control field when desired. In the dark-state polariton picture, the storage and retrieval process can be considered as a coherent conversion between the optical field and atomic spin wave [22]. However, even if the control field is nonadiabatically (instantly) turned on and off, the additional energy loss is in the order of v_g/c , which is very small for most situations [23,24]. In the storing process, one needs to select a suitable Ω_c such that the group velocity is slow enough and almost the whole probe pulse can be compressed into the media [17]. Also, the timing when the control field is turned off needs to be suitable, such that leakage at the front and rear tails of the probe pulse is minimized [17].

To quantify this leakage loss, we define an operational efficiency, termed F . Then, the overall storage efficiency (SE) of a memory can be estimated through the product of the transmission efficiency (TE) of the slow light and F , $SE = TE \times F$. We emphasize that there may exist additional losses during storage and retrieval processes and the storage period due to the finite γ_{sg} , which we set to zero for simplicity [24]. In order to compress almost the whole probe pulse into the atomic medium, it is necessary to choose a suitable Ω_c smaller than a certain value [and thus η is larger than a certain value denoted by η_{store} obtained through Eq. (13)] to enable F to approach unity. Fig. 2(b) depicts the relationship between the TE and η_{store} for some given F 's ($F = 95.5\% - 99.5\%$). For a smaller optical depth and thus a smaller TE, the broadening effect is more severe [17] such that η_{store} needs to be larger to minimize the tail leakage. More quantitative details about how to calculate these curves are described in the Appendix. We are only concerned with the high TE cases, e.g., $TE \gtrsim 80\%$. In those cases, η_{store} has a weak dependence on TE in order to maintain a fixed F of near unity. In other words, one may keep η_{store} roughly constant (around 2–3) to maintain a given small leakage loss. Although TE is actually dependent on D , we plot the curves of constant F versus TE but not D because it allows one to directly estimate the SE by the product of TE with F .

The results for calculation of the slow light transmission using Eq. (15) versus the probe bandwidth (B) under the constraint of $\eta = 2.43$, which corresponds to $F \approx 98.5\%$, are shown in Fig. 2(c). The storage efficiency is thus mainly determined by TE with an uncertainty of less than 1.5%. From Fig. 2(c), we can see that, for smaller B 's, TE is nearly constant with its value depending on the optical depth (D). With a larger D , the bandwidth of the constant TE extends to a wider value, roughly proportional to $\sqrt{D}\Gamma$. This trend of nearly constant TE below a certain bandwidth is understandable and is explained below. If the probe bandwidth is in the intensity-linear regime, following Eqs. (8) and (13), η can be rewritten as $\eta \propto \sqrt{D} \frac{B}{\Delta\omega_{EIT}}$. For a fixed η and a fixed D , the ratio of the pulse bandwidth to the EIT bandwidth is fixed such that the slow light transmission stays constant. From Fig. 2(c), one can also observe that the bandwidth range of the TE plateau is larger for a larger D . With a constant η , a

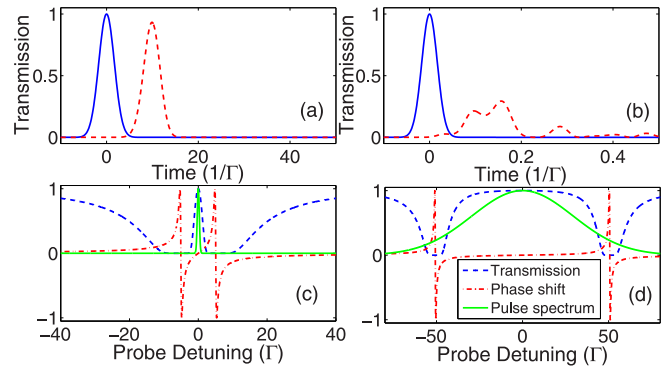


FIG. 3. (a) and (b) The input (blue solid) and output probe (red dashed) pulses with T_p of $4/\Gamma$ and $0.04/\Gamma$, respectively, for $D = 1000$ and $\eta = 2.43$. The transmission and waveform likenesses for the slow light pulse are 96.82% and 99.84% in (a) and 84.85% and 39.30% in (b), respectively. The EIT transmission spectrum, phase shift, and probe pulse spectrum, corresponding to the parameters used in (a) and (b), are plotted in (c) and (d), respectively. The maximum phase shift is normalized to unity for clarity.

larger D means that the ratio $\frac{B}{\Delta\omega_{EIT}}$ is smaller. Therefore, more frequency components of the probe pulse lie in the central region of the EIT transparent window, which leads to a larger transmission.

As can be seen in Fig. 2(c), when the bandwidth of the probe pulse B increases further, the transmission drops and a dip structure appears and then increases toward unity. This dip structure appears when the pulse bandwidth is on the order of the spectral separation of the two Aulter-Townes absorption peaks, which is $\sim\Omega_c$, such that the probe absorption is at a maximum. For an even higher B , a significant portion of the pulse spectral component lies beyond the Aulter-Townes absorption peaks in the far-detuned and nearly transparent regime. Therefore, the transmission rises again. Although TE is high in this circumstance, the probe pulse experiences a severe distortion because the high order dispersion terms are not negligible. As an example, Fig. 3(a) and 3(b) depict the two slow light pulses obtained with T_p of $4/\Gamma$ and $0.04/\Gamma$, respectively, after passing through an EIT medium with $D = 1000$ and $\eta = 2.43$. Figures 3(c) and 3(d) depict the corresponding EIT transmission, phase shift and pulse spectrum. For the long pulse case, the spectrum is relatively narrow, within the transparent window. Also, the pulse spectrum lies in a spectral range of nearly linear phase shift dependence on the detuning. Thus, the group velocity is well defined, and the slow light pulse resembles the input pulse with a certain group delay. For the short pulse case, however, the spectrum extends over the two Aulter-Townes absorption doublets as well as falling within the complicated profile of the phase shift spectrum. The pulse not only experiences significant absorption but also significant dispersion leading to significant distortion of the output pulse. This serious distortion in the temporal mode may introduce some complications in quantum memory applications. In addition to the efficiency, it is necessary to define another figure of merit to quantify this distortion to evaluate the performance of an optical memory.

C. Waveform likeness

Based on the above discussion, we invoke a figure of merit, the waveform likeness (WL), to quantify the extent of pulse distortion, formulated as follows:

$$\text{WL} \equiv \frac{\left| \int_{-\infty}^{\infty} \Omega_{p,in}^*(t - T_d) \Omega_{p,out}(t) dt \right|^2}{\int_{-\infty}^{\infty} |\Omega_{p,in}(t)|^2 dt \int_{-\infty}^{\infty} |\Omega_{p,out}(t)|^2 dt}. \quad (16)$$

The waveform likeness reflects the similarity between the input and slowed (or retrieved) probe pulses. It has been mentioned in many papers, although a different term might be used [16–19]. We will explain later that it has a direct relation to the adiabaticity of the memory. Figure 2(d) depicts the WLs for different input pulse bandwidths, corresponding to the TE shown in Fig. 2(c). The severe pulse distortion at a high bandwidth can be manifested by degradation of the WL. For clarity, we do not show the WL below 50% in Fig. 2(d). Similar to the TE, there is a plateau for WL in the low B regime. For a larger D , this plateau extends over a wider range, but is slightly smaller than that of the TE. This suggests that the WL is a more stringent parameter than TE at a high pulse bandwidth.

As can be seen in Fig. 3(b) for the broadband case, the output pulse profile splits over a long period of time. Although the TE remains high (84.85%), the WL is very low (39.3%). This highlights the need to introduce the parameter WL. In the case illustrated in Fig. 3(b), the fragmentary signals needed to be collected over a long time window to maintain the desired SE. This may affect storage feasibility for quantum memory applications, especially in the single-photon regime since the noise makes it difficult to collect a signal over a long time window. In addition, the group delay is not well defined in the broadband case. A certain portion of the pulse is delayed with sufficient time but a front tail virtually without any delay exists. It is therefore not feasible to store the probe pulse with a negligible amount of leakage.

1. Broadband limit

The numerator in the definition of WL in Eq. (16) can be simplified to

$$\text{WL} \propto \left| \int d\omega |W_p(\omega, 0)|^2 e^{i(k_1(\omega)L - \frac{D\Gamma\omega}{\Omega_c^2})} \right|^2. \quad (17)$$

The expression $k_1(\omega)$ of Eq. (5) can be written as

$$k_1(\omega)L = \frac{D\Gamma}{\Omega_c^2} \frac{\omega}{1 - 2i\frac{\omega\Gamma}{\Omega_c^2} - \frac{4\omega^2}{\Omega_c^2}}. \quad (18)$$

In the broadband EIT memory regime, the condition $B \gg \Gamma$ is valid. With the EIT memory protocol, the condition $B < \Delta\omega_{\text{EIT}} < \Omega_c$ is valid. Therefore, $\Omega_c > B \gg \Gamma$, and we have $\frac{\Gamma}{\Omega_c} \ll 1$ and $\frac{B}{\Omega_c} < 1$. By replacing ω by the pulse bandwidth B , the term $2\frac{\omega\Gamma}{\Omega_c^2}$ in the denominator of Eq. (18) is thus much smaller than unity and can be neglected. In this situation, $k_1(\omega)$ is almost a real number and reads as follows:

$$k_1(\omega)L \simeq \frac{D\Gamma\omega}{\Omega_c^2 - 4\omega^2}. \quad (19)$$

Thus, the transmission efficiency of the output probe pulse is near unity, as can be seen from Eq. (15) because $\text{Im}[k_1(\omega)]$

is near zero. This is understandable since the EIT transparent window is very wide and has a flat-top profile in the broadband regime, as shown in Fig. 3(d). If $B \ll \Omega_c$, almost all the pulse spectrum lies in the near-unity transparent window, which leads to a near-unity transmission.

Because WL is actually determined by the relative interplay between W_p and $k_1(\omega)$, we can consider all spectral behaviors to be normalized to B . We define $\tilde{k}_1(\tilde{\omega}) = k_1(\tilde{\omega}B)$ and $\tilde{W}_p(\tilde{\omega}) = W_p(\tilde{\omega}B)$, where $\tilde{\omega} = \frac{\omega}{B}$. Considering the different bandwidth B , $\tilde{W}_p(\tilde{\omega})$ remains the same and the WL of the spectral integral Eq. (17) is determined by $\tilde{k}_1(\tilde{\omega})$ alone, which reads

$$\tilde{k}_1(\tilde{\omega})L = \frac{D\Gamma}{B} \frac{\tilde{\omega}}{\left(\frac{\Omega_c}{B}\right)^2 - 4\tilde{\omega}^2}. \quad (20)$$

Here, we introduce two parameters: ξ_c and ξ_D , defined as

$$\begin{aligned} \xi_c &\equiv \frac{\Omega_c}{B}, \\ \xi_D &\equiv \frac{D\Gamma}{B}. \end{aligned} \quad (21)$$

Therefore, Eq. (20) can be rewritten as

$$\tilde{k}_1(\tilde{\omega})L \approx \xi_D \frac{\tilde{\omega}}{\xi_c^2 - 4\tilde{\omega}^2}. \quad (22)$$

If we keep the same values for ξ_c and ξ_D when varying B , the normalized response $\tilde{k}_1(\tilde{\omega})L$ can be maintained exactly at the same value by adjusting Ω_c and D according to Eq. (21) with $\Omega_c = \xi_c B$ and $D = \xi_D \frac{B}{\Gamma}$. Since the same WL is maintained for the normalized spectrum, it is the values of ξ_c and ξ_D which determine the criterion for the waveform likeness. These two parameters connect to η by $\eta = \frac{1}{4\ln(2)} \frac{\xi_D}{\xi_c^2}$. For simplicity, hereafter, we consider ξ_c and η as the two independent variables, while ξ_D can be determined based on the other two parameters. Thus, the whole picture of WL in the broadband limit can be summarized by η and ξ_c . It should be pointed out that ξ_c denotes the ratio of the EIT bandwidth (in the strong control limit) to the bandwidth of the input probe pulse. Conceivably, a larger ξ_c means that the probe spectrum is well located in the central EIT window, which results in a high WL.

Note that once (ξ_c, η) is fixed, WL converges to a constant value in the large bandwidth limit, as depicted in the example of Fig. 4(a). A numerical simulation of the convergent WL for different (ξ_c, η) with a given large B of 880Γ is shown in Fig. 4(b). In the broadband EIT regime, one can use the information in Fig. 4(b) to determine the WL and estimate the required experimental parameters (D, Ω_c) by Eq. (21). In other words, under the condition of $B/\Gamma \gg 1$, all information about WL has been mapped in Fig. 4(b). The trend of WL is easily captured in Fig. 4(b): decreasing η and increasing ξ_c is favorable to WL. However, there is a minimum requirement for η such that the storage of almost the whole pulse is possible. For a fixed η of 2.5, WL is determined solely by ξ_c , as depicted in Fig. 4(c). In the high-WL condition, the pulse distortion mainly comes from the third-order dispersion term. Under such a condition, the approximate analytical form for

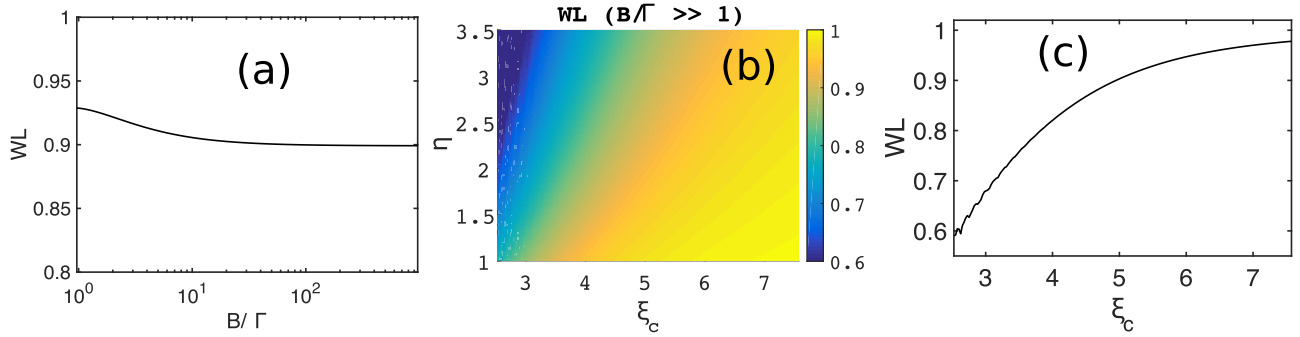


FIG. 4. (a) Solid curves denoting the WLs simulated with different bandwidths with fixed $(\xi_c, \eta) = (5.18, 2.77)$. (b) WLs for different (ξ_c, η) when $B/\Gamma \gg 1$. In the simulation, $B/\Gamma = 880$. Note that WL will converge to the value in this figure in the broadband limit. (c) Cross section of (b) along the ξ_c axis for $\eta = 2.5$.

WL ≈ 1 can be obtained by

$$\text{WL} \approx \left[1 - 5.4 \times \left(\frac{\eta}{\xi_c^2} \right)^2 \right]^2. \quad (23)$$

With a given parameter set of (ξ_c, η) , the approximate WL is also determined.

2. Adiabatic storage

Experimentally, the three variable parameters are D , Ω_c , and T_p (or B). By putting the relation of ξ_c into that of η and reducing Ω_c , one gets

$$DT_p\Gamma = \eta\xi_c^2 \times [4 \ln(2)]^2. \quad (24)$$

In Ref. [10], the parameter $DT_p\Gamma$ has been identified as a measure of degree of adiabaticity in EIT storage, with a larger value indicating a higher degree of adiabaticity. Therefore, we term it the adiabaticity parameter. As mentioned before, the parameter η must be larger than a certain value (e.g., ~ 2.5) in order to store most of the probe pulse in the media. The adiabaticity parameter $DT_p\Gamma$ is thus mainly determined by ξ_c . Once both η and ξ_c are determined, the adiabaticity parameter can be directly link to WL through Eq. (23). Due to this direct connection, one can reverse the logic and consider WL as an experimentally observable parameter useful for evaluating the degree of adiabaticity of the memory.

The dashed line in Fig. 5(a) depicts an example of the calculated WL through Eq. (23) versus the adiabaticity parameter for $D = 1000$ and $\eta = 2.5$. The solid line indicates the WL

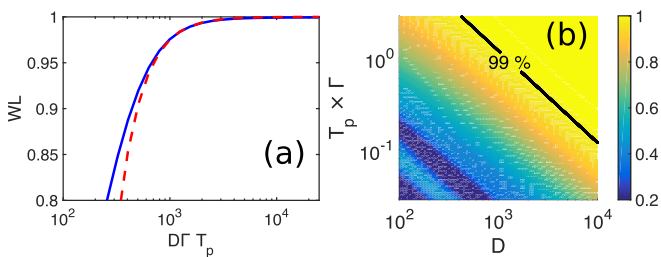


FIG. 5. (a) WL versus $DT_p\Gamma$. Here, we fix $D = 1000$ and vary T_p . The solid curve is based on the numerical simulation and the dashed curve is calculated through Eq. (23). (b) WL as a function of T_p and D in logarithmic-logarithmic scale. In both graphs, $\eta = 2.5$ is assumed.

obtained from the numerical calculation. The analytic formula matches the numerical calculation at high WLs but shows some deviation at lower WLs. Fig. 5(b) depicts the numerical calculation of the two-dimensional contour plot of WL versus $T_p\Gamma$ and D for $\eta = 2.5$. It is evident that the WL is nearly constant for a constant product of $DT_p\Gamma$, which is expected as mentioned above.

In comparison with the ATS protocol [12,13], which utilizes the nonadiabatic process to convert the polarization coherence into spin coherence, the value $DT_p\Gamma$ is located between 1 and 100, and therefore the WL is not high. In the ATS protocol, pulse distortion comes from the oscillation between the polarization and spin coherence and one extracts one of the pulses but not all of the photonic signal in the temporal domain. If one only focuses on the extracted pulse, it is not severely distorted but retains a Gaussian shape [12,13]. However, there is certainly a sacrifice in efficiency. In the EIT protocol, all optical signals in the temporal domain are included in the evaluation of WL. It is possible to reach a high WL and a high SE simultaneously for adiabatic EIT storage. However, there is a high demand for D and Ω_c , which will be discussed below.

D. Experimental requirements

In this section, we provide a guide on the required optical depth D and control intensity (characterized by Ω_c) when implementing a broadband EIT memory with values of SE and WL above a given threshold. Figures 6(a) and 6(b) depict two representative examples of TE and WL versus D for the narrowband and broadband cases, with B/Γ of 0.277 and 693.15, respectively, with $\eta = 2.5$ to satisfy the storage requirement. In the narrowband case, the WL is larger than the TE, while the situation is the opposite for the broadband case. In other words, TE (WL) is the bottleneck for the operation of the narrowband (broadband) EIT storage. From many of these plots of different bandwidth (B), one can plot WL (or TE) versus B under the condition that TE (or WL) is kept at a given fixed value. As one representative example, Fig. 6(c) [6(d)] depicts WL (TE) versus B for TE (WL) kept at a fixed value of 0.9 (red circles) and 0.8 (blue squares). From Fig. 6(c), it can be seen that WL (TE = 0.9) or WL (TE = 0.8) is larger than 0.9 or 0.8, respectively, for B smaller than a certain value (denoted as B_M) of $\approx 2.5\Gamma$. For $B > B_M$, WL of a given fixed

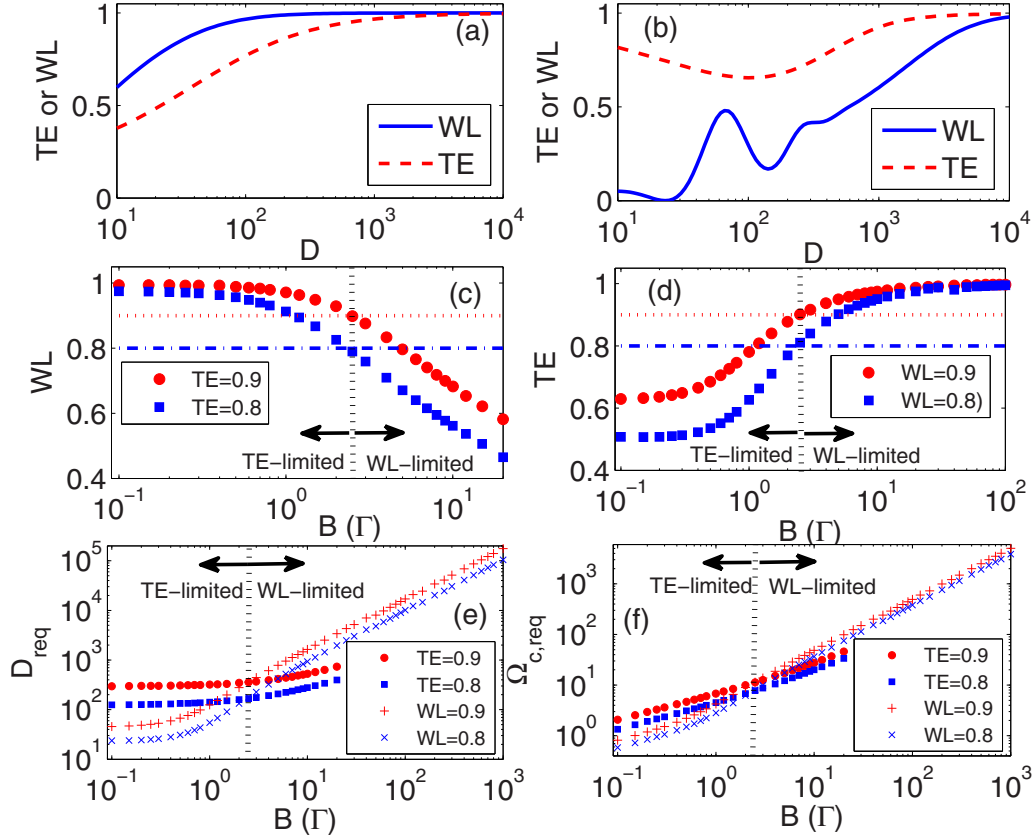


FIG. 6. (a) and (b) depict the TE and WL versus D for a given T_p (or B) with $T_p\Gamma = 10$ and 0.004 or $B/\Gamma = 0.277$ and 693.15 , respectively. Here, Ω_c is determined by the relation $\eta = 2.5$. (c) Red circles (blue squares) depict WL versus B for TE fixed at 0.9 (0.8). (d) Red circles (blue squares) depict TE versus B for WL fixed at 0.9 (0.8). Red dotted (blue dash dotted) lines indicate the y-axis value of 0.9 (0.8) in (c) and (d). The black dotted line at $B = B_M \approx 2.5\Gamma$ divides the EIT storage into two regimes: TE-limited ($WL > TE$) and WL-limited ($TE > WL$) regime for $B < B_M$ and $B > B_M$, respectively. (e) The required optical depth (D_{req}) versus the bandwidth B . (f) The corresponding required $\Omega_{c,\text{req}}$ for D_{req} in (e). In (e) and (f), the red circles (blue squares) denote the required D and $\Omega_{c,\text{req}}$ needed to satisfy $TE = 0.9$ ($TE = 0.8$) and the red plus (blue cross) markers denote the D_{req} and $\Omega_{c,\text{req}}$ to satisfy $WL = 0.9$ ($WL = 0.8$). The blue dotted line in (e) and (f) indicates the boundary of the TE-limited and WL-limited regimes.

TE is smaller than that TE. The EIT storage is thus naturally divided into two regimes: the narrowband regime ($B < B_M$) which is TE limited and the broadband regime ($B > B_M$) which is WL limited. One can apply similar argument to the case of Fig. 6(d) and reach the same conclusion.

The corresponding D and Ω_c for the four conditions in Figs. 6(c) and 6(d) are plotted in Figs. 6(e) and 6(f), respectively. It is evident that the required optical depth (denoted as D_{req}) and control Rabi frequencies (denoted by $\Omega_{c,\text{req}}$) are constrained by TE or WL when $B \lesssim B_M$ or $B \gtrsim B_M$, respectively. A similar trend of the TE- and WL-limited regimes still holds if one chooses different threshold values for TE and WL, although the exact quantities D_{req} and $\Omega_{c,\text{req}}$ may change. In the memory application, one may want to obtain a TE and WL greater than a certain threshold value simultaneously (e.g., with $TE \geq 0.9$ and $WL \geq 0.9$ or another combination of the values of TE and WL). One can choose D and Ω_c greater than the larger ones among D_{req} and $\Omega_{c,\text{req}}$ of the two regimes constrained by TE or WL of the required threshold values. The behavior of TE-limited or WL-limited regime is related to the dispersion properties discussed in Sec. II B. Dispersion

up to $O(\omega^3)$ is needed to be considered for the broadband EIT memory regime ($B > \Gamma$), such that the pulse distortion and thus the WL are a bottleneck. In the narrowband regime, the Gaussian waveform is well preserved and WL is not the bottleneck but the TE is. This also explains why previous studies in narrowband EIT memories were not affected much by the distortion issue [16,17]. In contrast, pushing towards the broadband regime, one steps into the WL-limited regime so pulse distortion must be considered. As can be observed in Fig. 6(e), the required optical depth is linearly proportional to the bandwidth in the WL-limited regime. This trend is understandable if we look at Eq. (24) and modify it to

$$D_{\text{req}} = 4 \ln(2) \eta \xi_c^2 \frac{B}{\Gamma}. \quad (25)$$

From Figs. 6(e) and 6(f) it is clear to see that, using the EIT protocol, the required D and Ω_c to achieve a high TE or WL are very high. The required D and Ω_c for a fixed WL are greater than those required for a fixed TE. For example, for a B of $\sim 20\Gamma$, $D \sim 740$ (3400) and $\Omega_c \sim 50$ (100) are required for a TE (WL) of ≥ 0.9 . The corresponding values of WL

and TE for $TE = 0.9$ and $WL = 0.9$ are 0.465 and 0.988, respectively. Experimentally, an optical depth greater than 10^3 has been achieved for cold atoms in free space [25] or in a hollow-core fiber [26]. An effective optical depth of 7600 has been achieved with cold atoms inside a cavity [27].

Broadband EIT memory requires a high optical depth and a strong control intensity; it is expected that some complicated effects may appear in real world situations which are beyond the scope of this paper. For example, nonlinear optical effects such as the photon switching effect due to off-resonant excitation of the coupling field to the nearby transition [28,29] or four-wave mixing [30] may become serious issues, although these effects can be reduced with some existing methods [17]. The influence of cooperative effects due to the resonant dipole-dipole interaction on the EIT memory could also become significant and warrant further study [17]. With these theoretical considerations in mind, we now present our experimental results towards achieving broadband EIT memory.

III. EXPERIMENTAL SETUP

A cesium magneto-optical trap (MOT) with a cigar-shaped atomic cloud is utilized to implement the EIT-based optical memory. To increase the optical depth of the atomic media, we employ a temporally dark and compressed MOT, as well as Zeeman-state optical pumping [25]. Pumping the population towards the single Zeeman substate ($|F = 3, m = 3\rangle$) also makes the storage performance less sensitive to stray magnetic fields [17,31], which is desirable for long-time storage. Efforts are made to reduce the ground-state decoherence rate γ_{gs} , such as minimizing the stray dc and ac magnetic fields and using the near copropagating probe and control beams to reduce the residual Doppler broadening. Details of the MOT setup can be found in [17,25].

The EIT optical memory is operated at the D_1 line with the probe beam driving the $|F = 3\rangle \rightarrow |F' = 4\rangle \sigma^+$ transition and the control beam driving the $|F = 4\rangle \rightarrow |F' = 4\rangle \sigma^+$ transition, as shown in Fig. 7(a). As pointed out in [17], operating the EIT at the D_1 transition can reduce the control-intensity-dependent ground-state decoherence rate due to the off-resonant excitation of the control beam to the nearby transition. A detailed plot of the setup appears in Fig. 7(b). The probe beam from the laser source passes twice through one acousto-optic modulator (AOM1) to adjust the frequency with minimal spatial movement. It is then sent to another AOM (AOM2) to be switched into a 160-ns square pulse. The probe beam is then coupled into a fiber electro-optic modulator (EOM) to shape the probe pulse into a Gaussian waveform with a full width at half maximum (FWHM) larger than 10 ns. Due to the finite extinction ratio (~ 18 dB) of the fiber EOM, AOM2 is added as an additional switch to minimize the probe leakage during storage. The probe beam is then coupled to the control beam through a 50 : 50 beam splitter. Both beams are sent into the cold atomic ensembles. Before entering the MOT cell, the probe beam is focused by a lens (L1) to an intensity e^{-2} diameter of $\sim 100 \mu\text{m}$ around the atomic cloud while the coupling beam is collimated by the same lens (L1) to a diameter of $\sim 240 \mu\text{m}$. After leaving the MOT cell, the control beam is focused by another lens (L2) and then blocked by a black dot. The probe beam, on the other hand, is collimated

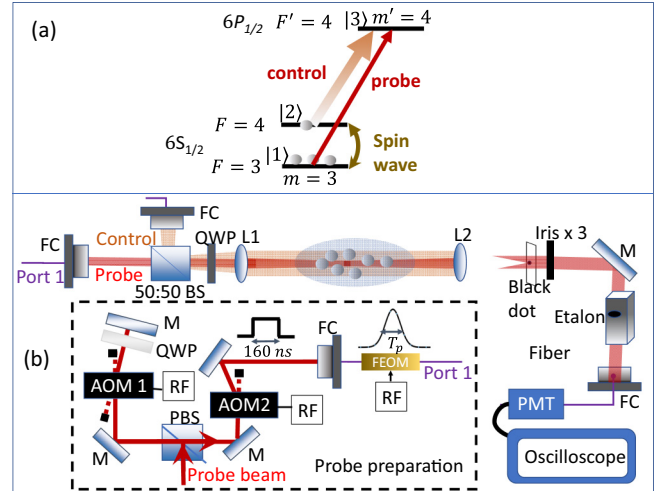


FIG. 7. (a) Energy levels and laser excitations of ^{133}Cs for EIT memory. (b) Experimental setup for EIT memory. AOM: acousto-optic modulator; BS: beam splitter. FEOM: fiber electro-optic modulator; RF: radio-frequency signal; PMT: photomultiplier tube; M: mirror; L: lens; QWP: quarter-wave plates; FC: fiber coupler; Port 1 is the transmitted probe beam through a polarized-maintaining fiber.

by the lens L2 and then coupled into a fiber before passing through three irises and an etalon filter, to filter out unwanted control light upon detection. The probe beam is then detected by a photomultiplier tube (Hamamatsu R636-10).

IV. RESULTS AND DISCUSSION

Here, we present our experimental results on broadband storage using the EIT protocol. We first discuss the efficiency versus the optical depth at a fixed temporal width for the input probe pulse. Then we vary the temporal width (or bandwidth) of the input probe pulse and study the efficiency dependence. Finally, we study the efficiency dependence on the storage time.

A. Efficiency dependence on optical depth

In a previous work [17], we studied the storage efficiency versus the optical depth for probe pulses of $T_p = 200$ ns. The storage is in the narrowband regime because the pulse bandwidth $B = 2\pi \times 2.2$ MHz is smaller than the spontaneous decay rate of $\Gamma = 2\pi \times 4.56$ MHz. To enter the broadband regime, we first consider the storage of probe pulses with a T_p of 30 ns, corresponding to a bandwidth of $B = 2\pi \times 14.71$ MHz. We then vary the optical depth (D) and adjust the control intensity for each D to obtain an optimized efficiency. Representative raw data showing the input, slowed, and stored-then-retrieved probe pulses are shown in Fig. 8(a). In this case, the parameters D and Ω_c are $392(46)$ and $16.48(0.23)\Gamma$, respectively, where the quantities shown in parentheses are the 2σ standard deviation. The Ω_c is determined by the spectral separation of the Autler-Townes splitting in the EIT spectrum, taken at a low optical depth (e.g., $D < 3$), such that the Autler-Townes doublets are clear. The optical depth is determined by the spectral fitting of the

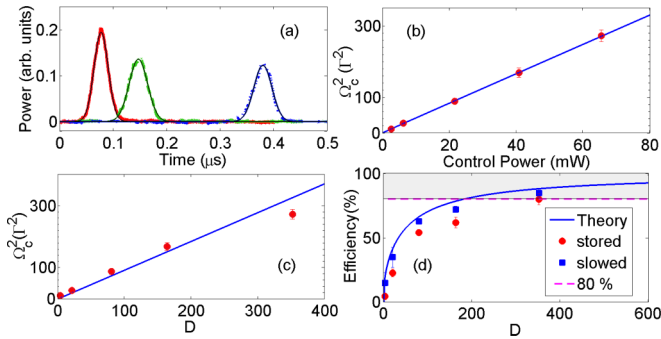


FIG. 8. (a) From left to right, the red solid, green dashed, and blue dotted curves represent the input, slowed (efficiency 86.1%), and stored-and-retrieved (efficiency 82.0%) probe pulses, respectively. The Gaussian fitting curves for each corresponding pulse are also shown (black solid lines). The parameters D and Ω_c are 392(46) and 16.48(0.21) Γ , respectively. (b) Ω_c^2 versus the control power. The solid blue line shows the linear fit to the data. (c) The optimum Ω_c^2 which maximizes the efficiency versus the optical depth. The blue solid line indicates the linear fit to the data. (d) The efficiencies of the slowed (blue squares) and stored-and-retrieved (red circles) probe pulses versus the optical depth. The solid blue line indicates the theoretically calculated slow light efficiency, assuming $\gamma_{ge} = 0$, $\gamma_{ge} = 0.75\Gamma$, and $\eta = 2.5$.

probe transmission spectrum with the control field off. In the fitting, we set $\gamma_{ge} = 0.75\Gamma$, which takes the finite laser linewidth and the laser frequency fluctuation into account [17].

As a consistency check of the determined Ω_c , the optimized Ω_c^2 for each D versus the control power, is shown in Fig. 8(b). As expected, the data fit a linear relation very well. Figure 8(c) depicts the optimized Ω_c^2 versus D , which reasonably follows a linear relation. This is expected since η is chosen to be nearly a constant to obtain the optimized efficiency. Due to Eq. (13), this implies that Ω_c^2 is linearly proportional to D for a fixed T_p . However, there is a slightly deviation from the linear relation in Fig. 8(c) for the data with the highest D . We speculate that it maybe due to the cooperative effect by resonant dipole-dipole interaction [32]. In our previous study [17], the cooperative effect is incorporated into the broadening of γ_{ge} , which is more significant for a higher D . In the current work, we assume γ_{ge} to be a constant for all D 's in the determination of D by spectral fitting. This may overestimate the optical depth, especially for a larger one. If that is true, the data point for the highest D may shift slightly to the left side, making the trend closer to a linear relation. However, the role of cooperative effect in EIT memories certainly deserves a more systematic study.

The corresponding efficiencies of the slowed and stored-then-retrieved probe pulses, determined by the ratio of the probe pulse energies with and without the presence of cold atoms, are indicated by the blue squares and red circles in Fig. 8(d), respectively. The blue solid line indicates the theoretical slow light efficiency with $\gamma_{ge} = 0.75\Gamma$ and $\eta = 2.5$. The theoretical curve matches the slow light efficiency well. At the highest D of 392(21), the achieved efficiency of the stored-then-retrieved pulse is 79.7(1.5)%.

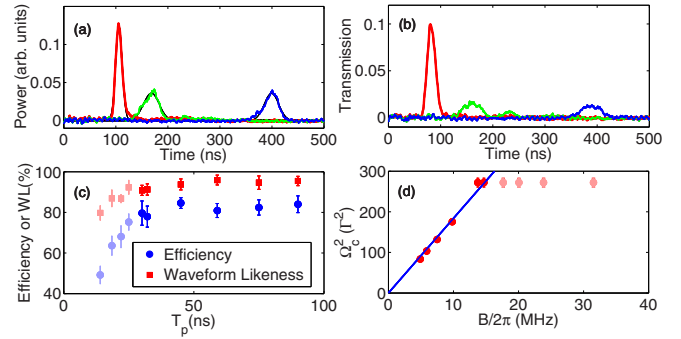


FIG. 9. From left to right, the red, green, and blue curves in (a) and (b) represent the input, slowed, and stored-and-retrieved probe pulses, respectively. (a) One representative example of the raw data with $T_p = 14$ ns, $D = 356(48)$, and $\Omega_c = 17.37(0.27)\Gamma$. The efficiency and waveform likenesses for the stored-then-retrieved pulse are 54.8% and 79.7%, respectively. (b) One representative example of the data to demonstrate the distortion in the slow light pulse. In this case, the parameters $\{T_p, D, \Omega_c\}$ are {18.6 ns, 123, 8.3 Γ }, respectively. The efficiency and WL for the stored-then-retrieved pulse are 31.8% and 64.7%, respectively. (c) The efficiency (blue circles) and waveform likeness (red squares) versus the FWHM pulse duration. The data points for $T_p < 30$ ns shown with lighter colors are taken with nonoptimized Ω_c , due to the limitation in available control power. (d) The used Ω_c^2 versus the pulse bandwidth for the data corresponding to those in (c). Data points shown in a lighter color are taken with nonoptimized Ω_c . The blue solid line indicates the linear fit for the six data points with narrower bandwidth (or larger T_p).

B. Efficiency dependence on the temporal width

Keeping at a large D of 356(48), we then vary the value of T_p from large to small (or B from small to large) and adjust the Ω_c to obtain an optimized efficiency. Unfortunately, the control intensity is technically limited to a certain level [corresponding to $\Omega_c = 17.37(0.27)\Gamma$] such that when $T_p < 30$ ns we cannot obtain the optimized efficiency. The results are shown in Fig. 9(c). The corresponding Ω_c^2 versus B are shown in Fig. 9(d). In Figs. 9(c) and 9(d), data points shown with lighter colors are those taken with nonoptimized Ω_c . For $T_p > 30$ ns, the Ω_c^2 versus B show a good fit to a linear relation, which means that η is maintained at nearly a constant value. The corresponding efficiencies for $T_p > 30$ ns are essentially constant with a variation of less than $\pm 2\%$ when η is kept at a constant value. The efficiency goes down when $T_p < 30$ ns, due to the nonoptimized Ω_c . Based on the fitting curves for the input and retrieved probe pulses, we can calculate the waveform likeness. The WLs are indicated by the red squares in Fig. 9(c). With the current experimental parameters, the EIT storage is in the TE-limited regime such that WL is larger than TE. Figure 9(a) depicts the raw data for $T_p = 14$ ns with $\Omega_c = 17.37\Gamma$. Due to the nonoptimized Ω_c , the slowed and retrieved pulses have a significant broadening which leads to a reduced WL. In Fig. 9(b), we show an example with significant pulse distortion or even splitting in the slowed pulse, in which $B < \Delta\omega_{\text{EIT}}$ is not satisfied. It is not surprising that both the efficiency and WL of the retrieved pulse are low in such a situation, being 31.8% and 64.7%, respectively.

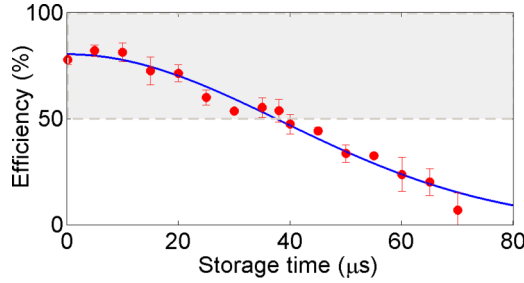


FIG. 10. Efficiency versus the storage time. The blue solid line indicates the fitting curve to the data with the fit function Ae^{-t/τ^2} , where the fitting parameters are $A = 80.3(3.8)\%$ and $\tau = 54.5(3.4) \mu\text{s}$. The grey dashed line represents the 50% efficiency.

C. Storage time

We now study the efficiency versus the storage time with $T_p = 30$ ns input pulses. The stray magnetic field is minimized to ~ 5 mG level by prolonging the storage time through three pairs of compensation coils [17]. Figure 10 shows an example of efficiency versus the storage time up to $70 \mu\text{s}$, which behaved like a Gaussian-decay function. This suggests that the atomic motion is the dominating decoherence mechanism in our system. The data are fit to a curve of Ae^{-t/τ^2} with the fitting parameters $A = 80.3(3.8)\%$ and $\tau = 54.5(3.4) \mu\text{s}$ [33]. The time-bandwidth product (TBP), defined as the ratio of the storage time at 50% efficiency to the FWHM input pulse duration (T_p), is an important figure of merit in quantum memory applications. The determined TBP for Fig. 10 is 1267(89), slightly higher than the 1200 obtained in our previous work with $T_p = 200$ ns [17]. The storage time may still be limited by the residual magnetic field and the residual Doppler broadening due to the atomic motion and the finite angle ($\sim 1^\circ$) between the probe and control beams [33].

V. CONCLUSION

In summary, we explore the EIT-based memory towards the broadband regime. The requirements for high-performance broadband EIT memory are theoretically discussed. A high optical depth and a strong control field are necessary to obtain the high-performance storage for short pulses, and the waveform likeness becomes the limitation in the broadband regime. We experimentally demonstrate the broadband EIT memory with a storage efficiency of $\sim 80\%$ (WL = 92.6%) for a 30-ns pulse and of $>50\%$ (WL = 79.7%) for a 14-ns pulse ($B = 31.4$ MHz). The achieved time-bandwidth product is 1267(89). Our work clarifies that it is possible to obtain high-efficiency and high-bandwidth adiabatic EIT memory, given a high optical depth and a strong control intensity.

Based on the calculation in Sec. IID and the achieved optical depth of ~ 1000 [17,25], we expect to obtain a bandwidth of ~ 100 MHz with an efficiency of $\sim 90\%$ if we could increase the control intensity by about a factor of 10, which is feasible if we use the tampered amplifier with an output power of a few watts for the control field. However, under such a condition, the waveform likeness is still relatively low (~ 0.5). If one also wants to achieve a WL of >0.9 , the required control intensity is about two times stronger and the required

optical depth is >3000 , which is beyond the capability of our current system. We note that an effective optical depth of ~ 7600 has been achieved in the system with cold atomic ensemble in an optical cavity [27].

ACKNOWLEDGMENTS

This work was supported by Ministry of Science and Technology of Taiwan under Grants No. 108-2112-M-001-030-MY3, No. 108-2639-M-007-001-ASP, and No. 109-2639-M-007-002-ASP. We also thank the support from NCTS ECP1.

APPENDIX: LEAKAGE-INDUCED LOSS

In the Appendix, we consider the relation between the choice of the parameter η and the optimized operational efficiency F due to pulse leakage during the storage process for a given transmission efficiency (TE) of the slow light pulse, as plotted in Fig. 2(b). We assume that EIT storage is in the regime where dispersion up to $O(\omega^2)$ is a good approximation. As mentioned in the [17], the slow light pulse is broadened by a factor of β and the relation $\text{TE} = \frac{1}{\beta}$ is satisfied in the ideal limit of $\gamma_{gs} = 0$. The overall operating efficiency F is the product of two terms, F_i and F_o , due to the leakage of the front and rear tails of the pulse, respectively [17]:

$$\begin{aligned} F_i &= \frac{1}{2}[1 + \text{erf}(2\sqrt{\ln(2)}\kappa)], \\ F_o &= \frac{1}{2}[1 + \text{erf}(2\sqrt{\ln(2)}(\eta - \kappa)/\beta)], \\ F &= F_i \times F_o. \end{aligned} \quad (\text{A1})$$

Here, κ denotes the ratio of the turned-off time of the control field (T_c) to the temporal width of the input pulse, i.e., $\kappa \equiv \frac{T_c}{T_p}$.

To search for the optimal κ that minimizes the leakage-induced loss, take the derivative of F with respect to κ ,

$$\begin{aligned} \partial_\kappa F &= e^{-(2\sqrt{\ln(2)}\kappa)^2} \left\{ \frac{1}{2}[1 + \text{erf}(2\sqrt{\ln(2)}(\eta - \kappa)/\beta)] \right\} \\ &\quad - \frac{1}{\beta} e^{-(2\sqrt{\ln(2)}(\eta - \kappa)/\beta)^2} \left\{ \frac{1}{2}[1 + \text{erf}(2\sqrt{\ln(2)}\kappa)] \right\} = 0. \end{aligned} \quad (\text{A2})$$

If the broadening is not too severe such that $\beta \simeq 1$, then when $\kappa = \frac{1}{\beta}(\eta - \kappa)$ the derivative is approximately zero. This assumption is valid if the TE is not much less than unity (see Sec. IIB). Under such an approximation, the optimized κ is

$$\kappa = \frac{\eta}{1 + \beta} = \frac{\eta}{1 + \frac{1}{\text{TE}}}, \quad (\text{A3})$$

and

$$F_i = F_o. \quad (\text{A4})$$

The operating efficiency is then,

$$F = F_i F_o = F_i^2, \quad (\text{A5})$$

with

$$F_i = F_o = \frac{1}{2}[1 + \text{erf}(2\sqrt{\ln(2)}\kappa)]. \quad (\text{A6})$$

- [1] F. Bussi eres, N. Sangouard, M. Afzelius, H. de Riedmatten, C. Simon, and W. Tittel, Prospective applications of optical quantum memories, *J. Mod. Opt.* **60**, 1519 (2013).
- [2] L.-M. Duan, M. D. Lukin, J. I. Cirac, and P. Zoller, Long-distance quantum communication with atomic ensembles and linear optics, *Nature (London)* **414**, 413 (2001).
- [3] K. F. Reim, J. Nunn, V. O. Lorenz, B. J. Sussman, K. C. Lee, N. K. Langford, D. Jaksch, and I. A. Walmsley, Towards high-speed optical quantum memories, *Nat. Photonics* **4**, 218 (2010).
- [4] K. F. Reim, P. Michelberger, K. C. Lee, J. Nunn, N. K. Langford, and I. A. Walmsley, Single-Photon-Level Quantum Memory at Room Temperature, *Phys. Rev. Lett.* **107**, 053603 (2011).
- [5] M. R. Sprague, P. S. Michelberger, T. F. M. Champion, D. G. England, J. Nunn, X.-M. Jin, W. S. Kolthammer, A. Abdolvand, P. S. J. Russell, and I. A. Walmsley, Broadband single-photon-level memory in a hollow-core photonic crystal fibre, *Nat. Photonics* **8**, 287 (2014).
- [6] D.-S. Ding, W. Zhang, Z.-Y. Zhou, S. Shi, B.-S. Shi, and G.-C. Guo, Raman quantum memory of photonic polarized entanglement, *Nat. Photonics* **9**, 332 (2015).
- [7] J. Wolters, G. Buser, A. Horsley, L. B egu in, A. J ockel, J.-P. Jahn, R. J. Warburton, and P. Treutlein, Simple Atomic Quantum Memory Suitable for Semiconductor Quantum Dot Single Photons, *Phys. Rev. Lett.* **119**, 060502 (2017).
- [8] R. Finkelstein, E. Poem, O. Michel, O. Lahad, and O. Firstenberg, Fast, noise-free memory for photon synchronization at room temperature, *Sci. Adv.* **4**, eaap8598 (2018).
- [9] J. Guo, X. Feng, P. Yang, Z. Yu, L. Q. Chen, C.-H. Yuan, and W. Zhang, High-performance raman quantum memory with optimal control in room temperature atoms, *Nat. Commun.* **10**, 148 (2019).
- [10] A. V. Gorshkov, A. Andr e, M. D. Lukin, and A. S. S orensen, Photon storage in Λ -type optically dense atomic media. II. Free-space model, *Phys. Rev. A* **76**, 033805 (2007).
- [11] W.-T. Liao, C. H. Keitel, and A. P alffy, All-Electromagnetic Control of Broadband Quantum Excitations Using Gradient Photon Echoes, *Phys. Rev. Lett.* **113**, 123602 (2014).
- [12] E. Saglamyurek, T. Hrushevskiy, A. Rastogi, K. Heshami, and L. J. LeBlanc, Coherent storage and manipulation of broadband photons via dynamically controlled Autler-Townes splitting, *Nat. Photonics* **12**, 774 (2018).
- [13] A. Rastogi, E. Saglamyurek, T. Hrushevskiy, S. Hubele, and L. J. LeBlanc, Discerning quantum memories based on electromagnetically-induced-transparency and Autler-Townes-splitting protocols, *Phys. Rev. A* **100**, 012314 (2019).
- [14] E. Saglamyurek, T. Hrushevskiy, L. Cooke, A. Rastogi, and L. J. LeBlanc, Single-photon-level light storage in cold atoms using the Autler-Townes splitting protocol, *Phys. Rev. Research* **1**, 022004 (2019).
- [15] D. D. Yavuz, Electromagnetically induced transparency with broadband laser pulses, *Phys. Rev. A* **75**, 031801(R) (2007).
- [16] Y.-H. Chen, M.-J. Lee, I.-C. Wang, S. Du, Y.-F. Chen, Y.-C. Chen, and I. A. Yu, Coherent Optical Memory with High Storage Efficiency and Large Fractional Delay, *Phys. Rev. Lett.* **110**, 083601 (2013).
- [17] Y.-F. Hsiao, P.-J. Tsai, H.-S. Chen, S.-X. Lin, C.-C. Hung, C.-H. Lee, Y.-H. Chen, Y.-F. Chen, I. A. Yu, and Y.-C. Chen, Highly Efficient Coherent Optical Memory Based on Electromagnetically Induced Transparency, *Phys. Rev. Lett.* **120**, 183602 (2018).
- [18] Y. Wang, J. Li, S. Zhang, K. Su, Y. Zhou, K. Liao, S. Du, H. Yan, and S.-L. Zhu, Efficient quantum memory for single-photon polarization qubits, *Nat. Photonics* **13**, 346 (2019).
- [19] S. Zhou, S. Zhang, C. Liu, J. F. Chen, J. Wen, M. M. T. Loy, G. K. L. Wong, and S. Du, Optimal storage and retrieval of single-photon waveforms, *Opt. Express* **20**, 24124 (2012).
- [20] T. Y. Abi-Salloum, Electromagnetically induced transparency and Autler-Townes splitting: Two similar but distinct phenomena in two categories of three-level atomic systems, *Phys. Rev. A* **81**, 053836 (2010).
- [21] Y.-F. Chen, Y.-M. Kao, W.-H. Lin, and I. A. Yu, Phase variation and shape distortion of light pulses in electromagnetically induced transparency media, *Phys. Rev. A* **74**, 063807 (2006).
- [22] M. Fleischhauer and M. D. Lukin, Dark-State Polaritons in Electromagnetically Induced Transparency, *Phys. Rev. Lett.* **84**, 5094 (2000).
- [23] A. B. Matsko, Y. V. Rostovtsev, O. Kocharovskaya, A. S. Zibrov, and M. O. Scully, Nonadiabatic approach to quantum optical information storage, *Phys. Rev. A* **64**, 043809 (2001).
- [24] P.-J. Tsai, Y.-C. Wei, B.-H. Wu, S.-X. Lin, and Y.-C. Chen, Theoretical study of a memory-based optical converter with degenerate Zeeman states, *Phys. Rev. A* **100**, 063843 (2019).
- [25] Y.-F. Hsiao, H.-S. Chen, P.-J. Tsai, and Y.-C. Chen, Cold atomic media with ultrahigh optical depths, *Phys. Rev. A* **90**, 055401 (2014).
- [26] F. Blatt, T. Halfmann, and T. Peters, One-dimensional ultracold medium of extreme optical depth, *Opt. Lett.* **39**, 446 (2014).
- [27] Y. Jiang, Y. Mei, Y. Zou, Y. Zuo, and S. Du, Intracavity cold atomic ensemble with high optical depth, *Rev. Sci. Instrum.* **90**, 013105 (2019).
- [28] H. Schmidt and A. Imamoglu, Giant Kerr nonlinearities obtained by electromagnetically induced transparency, *Opt. Lett.* **21**, 1936 (1996).
- [29] S. E. Harris and Y. Yamamoto, Photon Switching by Quantum Interference, *Phys. Rev. Lett.* **81**, 3611 (1998).
- [30] N. Lauk, C. O'Brien, and M. Fleischhauer, Fidelity of photon propagation in electromagnetically induced transparency in the presence of four-wave mixing, *Phys. Rev. A* **88**, 013823 (2013).
- [31] T. Peters, Y.-H. Chen, J.-S. Wang, Y.-W. Lin, and I. A. Yu, Optimizing the retrieval efficiency of stored light pulses, *Opt. Express* **17**, 6665 (2009).
- [32] S. Jennewein, M. Besbes, N. J. Schilder, S. D. Jenkins, C. Sauvan, J. Ruostekoski, J.-J. Greffet, Y. R. P. Sortais, and A. Browaeys, Coherent Scattering of Near-Resonant Light by a Dense Microscopic Cold Atomic Cloud, *Phys. Rev. Lett.* **116**, 233601 (2016).
- [33] B. Zhao, Y.-A. Chen, X.-H. Bao, T. Strassel, C.-S. Chuu, X.-M. Jin, J. Schmiedmayer, Z.-S. Yuan, S. Chen, and J.-W. Pan, A millisecond quantum memory for scalable quantum networks, *Nat. Phys.* **5**, 95 (2009).